analytical chemistry

ARTICLE

pubs.acs.org/ac

Bipolar Electrode Focusing: Faradaic Ion Concentration Polarization

Robbyn K. Anand, Eoin Sheridan, Kyle N. Knust, and Richard M. Crooks*

Department of Chemistry and Biochemistry, Center for Electrochemistry, and the Center for Nano- and Molecular Science and Technology, The University of Texas at Austin, 1 University Station, A5300, Austin, Texas 78712-0165, United States

Supporting Information

ABSTRACT: Bipolar electrode (BPE) focusing locally enriches charged analytes in a microchannel along an electric field gradient that opposes a counter-flow. This electric field gradient forms at the boundary of an ion depletion zone generated by the BPE. Here, we demonstrate concentration enrichment of a fluorescent tracer by up to 500 000-fold. The use of a dual-channel microfluidic configuration, composed of two microchannels electrochemically connected by a BPE, enhances the rate of enrichment (up to 71-fold/s). Faradaic reactions at the ends of the BPE generate ion depletion and enrichment zones in the two, separated channels. This type of device is equivalent to previously reported micro/nanochannel junction arrangements used for ion concentration polarization, but it is experimentally more flexible and much simpler to construct.

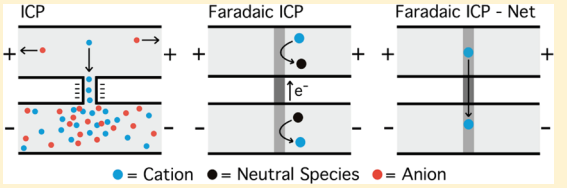

In this paper, we report the use of bipolar electrodes (BPEs) for focusing and concentrating analytes by up to 500 000-fold (Scheme 1)[1−5] and at a rate as high as 71-fold/s in a new dual-channel fluidic configuration (Scheme 2a). The dual-channel configuration decouples the applied driving voltage, which is required for focusing, from the potential drop across the BPE. We demonstrate that this leads to some important practical advantages for concentrating analytes. Additionally, we show that faradaic processes at a BPE spanning two fluidic channels can be used to generate ion depletion and enrichment zones that are analogous to those resulting from ion concentration polarization (ICP) at micro/nanochannel junctions. This is a significant finding, because the "faradaic ICP" method described here produces the same type of ion depletion zone as ICP but without the need for fabricating channels having nanometer-scale dimensions.

Lab-on-a-chip devices (LoCs) offer many opportunities for new sensing and sample processing strategies, including high resolution separation,[6,7] single-cell manipulation,[6,8] nanoscale transport investigation,[9,10] and microdroplet chemistry,[11,12] along with many others.[13] The advantages of LoC technologies lie in the characteristic micro- to nanoscale fluidic components, which enable precise handling of very small solution volumes (pL−nL), while also introducing transport phenomena unique to this size scale.[13] However, detection of analytes in LoCs can be challenging due to the combination of small detection volumes and low concentration of analytes frequently encountered. Therefore, local enrichment of analyte concentration in the detection volume is highly desirable.

Many methods have been developed to accomplish analyte enrichment in LoCs.[14] One of these was developed by us, and we refer to it as BPE focusing.[15] Briefly, BPE focusing is a counter-flow gradient focusing (CFGF) method in which electromigration velocity is balanced against a counter flow.[2,16] CFGF methods have in common a gradient in electric field strength along which each analyte focuses at a unique location based upon its electrophoretic mobility. CFGF methods fall under the broader category of electrokinetic equilibrium techniques, which also includes isoelectric focusing (IEF),[17−19] field amplified sample stacking,[20,21] and isotachophoresis.[22,23] Other CFGF methods include temperature gradient focusing (TGF),[24−26] electric field gradient focusing (EFGF),[27−32] and dynamic field gradient focusing (DFGF).[33−35]

If concentration enrichment, rather than separation, is the primary goal of a CFGF method, then the steepest possible local electric field gradient is desirable. Such a gradient can form at the boundary of a zone depleted of ions in an electrolyte-filled channel and indeed just such a depletion zone is produced at a micro/nanochannel junction in ICP.[36−39] This approach results in very rapid enrichment. For example, Wang et al. enriched 33 pM green fluorescent protein at a depletion zone boundary by 100 000-fold in just 60 min (28-fold/s).[38] The authors reported further enrichment, up to 10^7-fold in 40 min, using a lower initial concentration (33 fM) of green fluorescent protein.[38]

BPE focusing also enriches analytes at a depletion zone boundary, but in this case, the electric field gradient forms near a BPE (Scheme 1d). Previously, we reported using this approach to concentrate a fluorescent anionic tracer by a factor of ∼500.[1,4] Here, we report 500 000-fold enrichment of a tracer, present at an initial concentration of 10.0 pM, within 150 min (56-fold/s) using a BPE in a single microchannel. We also introduce a dual-channel arrangement, which leads to even more rapid enrichment, reaching 142 000-fold in ∼33 min (71-fold/s). These performance gains result from a better fundamental

Received: December 20, 2010
Accepted: January 31, 2011
Published: February 25, 2011

Scheme 1

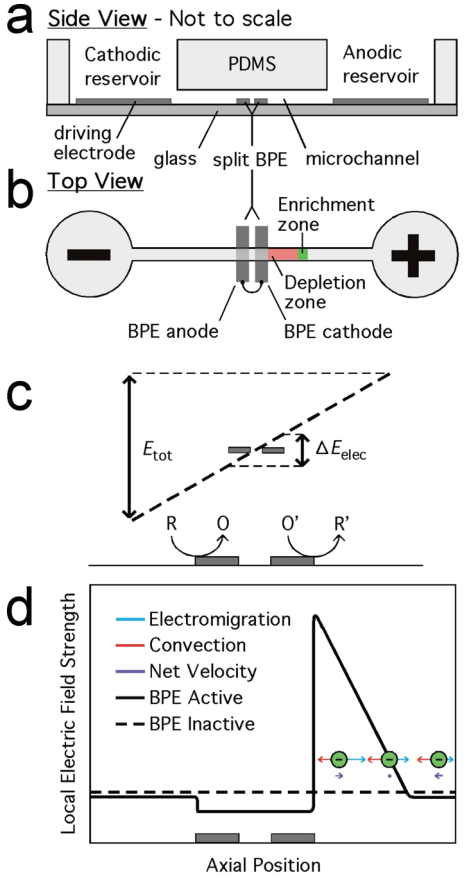

Scheme 2

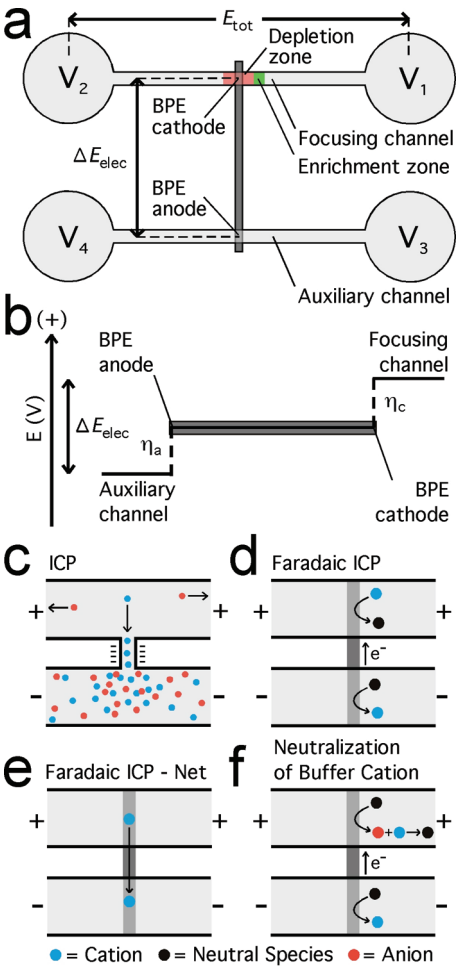

understanding of the experimental parameters affecting enrichment in BPE focusing. Specifically, a 12.5-fold reduction of the height of the microchannel relative to our previous fluidic design not only leads to reduction in Taylor dispersion[1,40] but also provides access to higher applied field strength and higher buffer concentration, both of which increase the slope of the electric field gradient (Scheme 1d).[1] The further performance gain observed in the dual-channel arrangement is due to decoupling of the driving voltage (E_{tot}) from the voltage drop over the BPE (ΔE_{elec}; Scheme 2a). This makes it possible to use higher values of E_{tot}, which in turn leads to enhanced enrichment. Finally, we show that the electric field gradient formed at a BPE is equivalent to that obtained at the micro/nanochannel junction in ICP.

EXPERIMENTAL SECTION

Chemicals. 4,4-Difluoro-1,3,5,7,8-pentamethyl-4-bora-3a,4a-diaza-*s*-indacene-2,6-disulfonic acid ($BODIPY^{2-}$, Molecular Probes, Eugene, OR) was used as a fluorescent tracer to quantitate the degree of concentration enrichment. A 0.5 M stock solution of Tris·$HClO_4$ (pH 8.1) was prepared from reagent grade Tris(hydroxymethyl)aminomethane (Sigma-Aldrich, Inc., St. Louis, MO) by dissolution in deionized water (18.0 MΩ·cm, Milli-Q Gradient System, Millipore) and subsequent titration with 2.0 N $HClO_4$ (Ricca Chemical Co., Arlington, TX). This stock solution was diluted to concentrations of 10.0 or 100.0 mM (pH 8.1) and used as background electrolyte. The silicone elastomer and curing agent (Sylgard 184) used to prepare the poly(dimethylsiloxane) (PDMS) microfluidic devices were obtained from K. R. Anderson, Inc. (Morgan Hill, CA).

Device Fabrication. The hybrid PDMS/glass microfluidic devices and Au electrodes were fabricated by a previously published procedure.[41] Briefly, microfluidic channels spanning two 4.0 mm-diameter reservoirs were fabricated from PDMS. The microchannels were 6.0 mm long and either 100 μm wide and 21 μm high or 10 μm wide and 1.6 μm high. Next, 100 nm-thick Au electrodes (no adhesion layer, Evaporated Metal Films, Ithaca, NY) were microfabricated on glass slides using standard photolithographic techniques. Finally, the PDMS and glass were exposed to an O_2 plasma (60 W, model PDC-32G, Harrick Scientific, Ossining, NY) for 15 s and then bonded together. The BPE was centered at the midpoint of the channel.

Two principal device configurations were used in this study. Single-channel focusing experiments and current measurements were carried out using a split, 100 μm-long BPE that spanned the width of the channel (Scheme 1a,b and Figure 1a). Each half of the BPE was 35 μm long, and there was a 30 μm gap between them. Leads from the two halves of the split BPE extended outside of the microchannel and could be connected externally by a conductive wire so that they acted like a single, 100 μm-long BPE.[5,42−44] This design allowed the current flowing through the BPE (i_{BPE}) to be measured by connecting the two halves of the electrode with an ammeter (Model 6517B electrometer, Keithley

dx.doi.org/10.1021/ac103302j |*Anal. Chem.* 2011, 83, 2351–2358

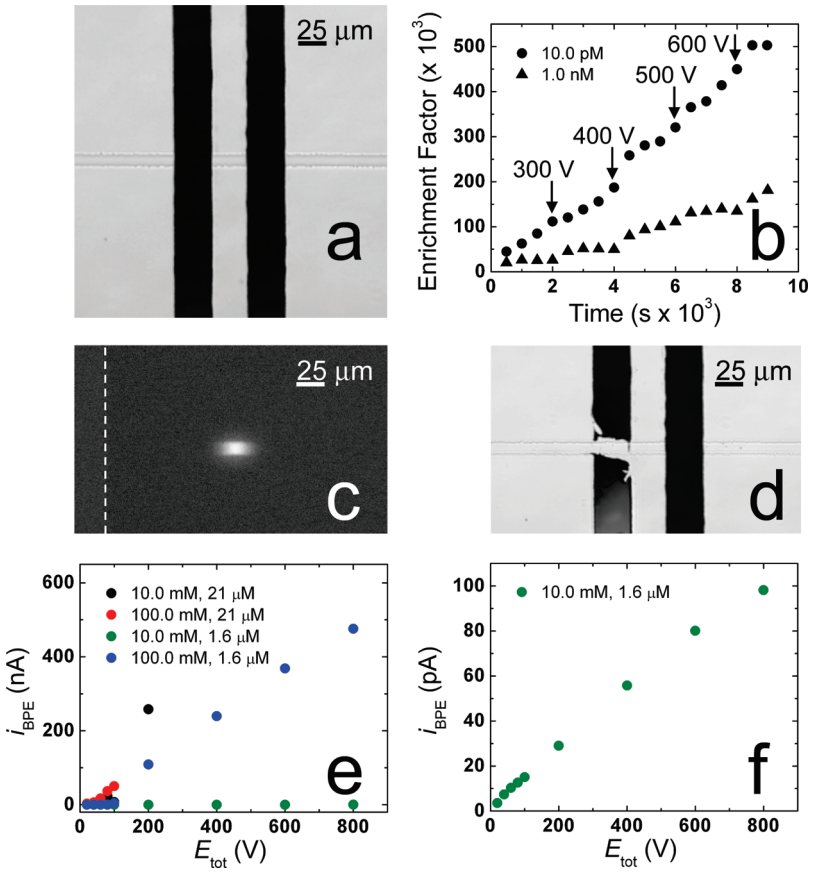

Figure 1. Optical micrograph of a 10 μm-wide, 1.6 μm-high PDMS microchannel crossing a 100 μm-wide split Au BPE (a) before and (d) after a 150 min enrichment experiment. (b) Enrichment factor (EF) as a function of time for initial $BODIPY^{2-}$ concentrations of 10.0 pM (circles) and 1.0 nM (triangles). The initial value of E_{tot} was 200 V, and it was increased by 100 V at 2000 s intervals (indicated by arrows). The electrolyte was pH 8.1, 100 mM Tris·$HClO_4$ buffer. (c) Fluorescence micrograph of an enriched band of the $BODIPY^{2-}$ fluorescent tracer (EF = ~30 000). The solution contained 1.0 nM $BODIPY^{2-}$ and 100 mM Tris·$HClO_4$ (pH 8.1). Enrichment was carried out for 1000 s at E_{tot} = 200 V. The dashed white line indicates the location of the cathodic edge of the BPE. (e and f) Plots of i_{BPE} versus E_{tot} for both a 100 μm-wide, 21 μm-high channel and a 10 μm-wide, 1.6 μm-high channel filled with either 10.0 mM or 100 mM Tris·$HClO_4$ (pH 8.1). These data were obtained using the 100 μm-wide split Au BPE.

Table 1. Voltage Patterns Applied for Dual-Channel Experiments

voltage pattern (VP)	V_1 (V)	V_2 (V)	V_3 (V)	V_4 (V)
1	50.0	ground	50.0	ground
2	200	ground	ground	ground
3	300	ground	50.0	50.0
4	35.0	ground	ground	ground

Instruments, Inc., Cleveland, OH). Driving electrodes consisted of a microfabricated Au electrode spanning the bottom of each reservoir (Scheme 1a). For dual-channel experiments, two 1.6 μm-high and 10 μm-wide channels, formed from two separate PDMS monoliths, were placed into electrochemical contact at their center with a 12.0 mm-long, 50 μm-wide BPE (Scheme 2a). Driving electrodes for the dual channel experiment consisted of a coiled Au wire immersed in each of the four reservoirs.

In addition to the two principal configurations described in the previous paragraph, two modified dual-channel devices were also used: one to measure the current through the BPE (i_{BPE}) and another to measure the difference in solution potential (ΔE_{elec}, Scheme 2b) between its ends. Schematics of the electrode configurations used for current and voltage measurements in the dual-channel configuration, along with experimental details of the measurements, are available in the Supporting Information.

Concentration Enrichment Experiments. Prior to each experiment, the microfluidic channel was rinsed with buffer (100.0 mM Tris, pH 8.1). In the single-channel configuration, this was carried out by applying E_{tot} = 50.0 V and allowing the buffer solution to flow through the microchannel for 5 min by electroosmosis. In the dual-channel configuration, four separate potentials (V_1, V_2, V_3, and V_4 in Scheme 2a) were applied using voltage pattern (VP) 1 (Table 1). Finally, the rinsing solution in each of the reservoirs of both device configurations was replaced with 40.0 μL of buffer containing either 10.0 pM or 1.0 nM $BODIPY^{2-}$.

Single-channel concentration-enrichment experiments were carried out by applying a driving voltage (E_{tot} = 200−600 V) across the microchannel using a custom-built power supply that incorporated a high-power, C-series voltage source (Ultra Volt, Ronkonkoma, NY) connected to the microfabricated Au driving electrodes spanning the bottoms of the reservoirs. For dual-channel experiments, concentration enrichment was carried out by applying the different VPs shown in Table 1. Simultaneously, the extent of enrichment was monitored by fluorescence microscopy.

Fluorescence Measurements. Enrichment of the $BODIPY^{2-}$ tracer dye was monitored using an inverted epifluorescence

dx.doi.org/10.1021/ac103302j |*Anal. Chem.* 2011, 83, 2351–2358

microscope (Eclipse TE 2000-U, Nikon) fitted with a CCD camera (Cascade 512B, Photometrics). Images were recorded at 5 or 10 s intervals and analyzed by image processing software (V++ Precision Digital Imaging, Digital Optics Limited, Auckland, New Zealand). Values of the enrichment factor (EF) were determined by dividing the maximum tracer concentration in the enriched band by the initial concentration. This was accomplished by comparing the region of maximum intensity in the concentrated band of dye to calibrated fluorescence intensities. All measurements were corrected for the background fluorescence intensity.

THEORY AND BACKGROUND

Ion Concentration Polarization at Micro/Nanochannel Junctions. Several excellent review articles have been published on the topic of ICP.[36,45,46] Briefly, for ICP to occur, ionic current flowing between two compartments, across which a potential bias is applied, must be carried by a significant majority of either cations or anions. In the case that cations are the majority charge carrier, a depletion zone forms in the anodic compartment and enrichment of both cations and anions occurs in the cathodic compartment (Scheme 2c). This scenario may be induced by connecting two microchannels by a nanochannel having walls with fixed negative charges. Counterions (cations in this case) screen the charge on the walls, forming an electrical double layer (EDL). If the EDLs on opposing walls overlap, then there will be selective transport of cations through the nanochannel. If however, the EDLs do not overlap, ionic current will be carried not only by cations through the EDL (i_{EDL}) but also by cations and anions through the bulk solution (i_b). In the latter case, ICP may still occur if a large majority of the current is carried through the EDL.[46] The magnitudes of i_{EDL} and i_b are determined by the EDL (σ_{EDL}) and bulk (σ_b) conductivities, respectively, and the ratio of these two conductivities is defined as the Dukhin number (D_u, eq 1).

$$D_u = \sigma_{EDL}/\sigma_b \quad (1)$$

Santiago and co-workers have shown that ICP is best characterized by an inverse Dukhin number ($1/D_u$), such that in the case of complete double layer overlap eq 2 applies.[46]

$$1/D_u = \sigma_b/\sigma_{EDL} = 0 \quad (2)$$

Comparison of Traditional ICP and Faradaic ICP between Two Microchannels. An important result reported here is that a BPE connecting two microchannels can also lead to ion depletion and enrichment zones by way of faradaic reactions. This situation is illustrated in Scheme 2d. Here, the reduction of a cation to a neutral species proceeds at the BPE cathode. The reverse process occurs at the BPE anode. These two processes, which must occur at the same rate to maintain electroneutrality, are equivalent to selective transport of cations from the anodic (+) microchannel to the cathodic (−) microchannel (Scheme 2e). This situation is analogous to perfectly selective cation transport through a negatively charged nanochannel (that is, $1/D_u = 0$) and can likewise result in the formation of ion depletion and enrichment zones in the anodic and cathodic microchannels, respectively. Importantly, the challenge of fabricating nanochannels is eliminated in faradaic ICP.

Despite the analogy between faradaic ICP and traditional ICP alluded to in the previous paragraph, there are also some important differences. First, the charge of ions generated and consumed (neutralized) at the ends of the BPE is determined by the nature of the faradaic reactions. For example, instead of "transporting" a cation from the anodic to cathodic microchannel, as shown in Scheme 2d,e, two different faradaic reactions could occur at the BPE ends. For example, a cation could be neutralized (reduced) at the BPE cathode while an anion could be neutralized (oxidized) at the BPE anode. In this case, the result would be generation of an ion depletion zone in each channel. This flexibility is significant, because it provides greater control over charge transport than traditional ICP. Second, the transport process is mediated by faradaic reactions. Therefore, unlike traditional ICP which is mass transport limited, faradaic ICP will be limited by electron-transfer kinetics if the faradaic reactions are slow. Third, the BPE introduces selectivity that is not available in traditional ICP. Specifically, a nanochannel transports ions based on charge (and size in the case of sterically hindered transport), while the BPE generates or neutralizes ions selectively on the basis of the interfacial potential and the reduction potential of the redox molecule. This selectivity requires that ΔE_{elec} be maintained at the magnitude necessary to drive the desired half reactions at the BPE ends. Finally, the BPE results in perfectly selective charge transport, which can only be approached in traditional ICP.

Faradaic ICP Mechanism. Scheme 2f depicts the reaction sequence used for faradaic ICP in the present study. Cations are generated by the oxidation of a neutral species at the BPE anode in the bottom channel of Scheme 2f. This is accomplished by water oxidation (eq 3).

$$2H_2O - 4e^- \rightarrow 4H^+ + O_2 \qquad E^o = 0.40\,V \quad (3)$$

Anions are generated by the reduction of neutral species at the BPE cathode (top channel). The anion then goes on to neutralize a buffer cation. The specific reactions are given by eqs 4 and 5, respectively.

$$2H_2O + 2e^- \rightarrow 2OH^- + H_2 \qquad E^o = -0.83\,V \quad (4)$$

$$OH^- + TrisH^+ \rightarrow Tris + H_2O \quad (5)$$

The net result of eqs 3−5 is the same as that shown in Scheme 2e: "transport" of a cation from the anodic to cathodic microchannel and corresponding formation of ion depletion and enrichment zones. Note that the rate of water electrolysis (eqs 3 and 4) is not limited by mass transfer but rather by electron-transfer kinetics. In this respect, the behavior of this particular faradaic ICP configuration is unlike traditional ICP in which the transfer of charge is limited by the rate of mass transfer of ions to the micro/nanochannel intersection. This difference is important, because it impacts the rate of formation of ion enrichment and depletion zones.

Faradaic ICP in a Single Microchannel. The previous two subsections addressed faradaic ICP with a BPE connecting two microchannels. This is analogous to traditional ICP with $1/D_u \rightarrow 0$. If the anodic and cathodic compartments are connected by both an electrolyte solution and a BPE, a situation arises which is analogous to traditional ICP where $1 > 1/D_u > 0$. That is, there is some bulk ionic conductance. We have previously observed that an ion depletion zone forms when a large majority of the total current flowing between the anodic and cathodic reservoirs (i_{tot}) passes through the BPE (i_{BPE}).[5] For example, an ion depletion zone forms at a 500 μm-long BPE situated at the center of a single microchannel having a uniform cross section (100 μm wide × 21 μm high) along its length (6.0 mm).[5] In this channel

geometry and under conditions in which a depletion zone formed, $i_{BPE}/i_{tot} \approx 0.8$.[5] In other words, in the segment of the microchannel containing the BPE, 80% of the current flowed through the BPE and 20% flowed through the electrolyte solution above it. This is analogous to ICP in which $i_{EDL}/(i_{EDL} + i_b) = 0.8$. This is significant, because such a dominance of i_{EDL} over i_b in traditional ICP requires a nanochannel. In contrast, the same effect is observed in a micrometer-scale channel outfitted with a BPE.

RESULTS AND DISCUSSION

BPE Focusing in a Single-Channel Configuration. Enrichment of the fluorescent tracer ($BODIPY^{2-}$) was carried out as follows in a 1.6 μm-high, single-channel device containing a 100 μm-long split BPE (Figure 1a). First, the channel was rinsed as described in the Experimental Section. Second, the buffer in the reservoirs was replaced with either 10.0 pM or 1.0 nM $BODIPY^{2-}$ in 100 mM Tris buffer (pH = 8.1). Finally, $E_{tot} = 200$ V was applied to initiate enrichment, and then, the driving voltage was increased by 100 V every 2000 s up to a maximum of 600 V. A fluorescence image of a typical enriched band (EF = 30 000 after 1000 s at $E_{tot} = 200$ V) is shown in Figure 1c.

Figure 1b shows the effect of voltage and time on the concentration enrichment of 10.0 pM and 1.0 nM $BODIPY^{2-}$ tracer. Tracer at an initial concentration of 10.0 pM enriches at an average rate of 56-fold/s reaching 500 000-fold enrichment in 150 min, while the 1.0 nM tracer enriches at 19-fold/s to 180 000-fold over the same period of time. During the course of these enrichment experiments, the Au BPE slowly degrades starting from its anodic edge (Figure 1d). This shortens the length of the BPE over which the solution potential is dropped, and this has the effect of gradually decreasing ΔE_{elec}. Electrode degradation can be prevented by enriching at lower E_{tot}, but the associated lower electric field strength and correspondingly shallower field gradient results in a lower EF.[1] Later, we will show that electrode degradation can also be avoided using the dual-channel configuration.

To maximize enrichment, E_{tot} was increased every 2000 s (indicated by arrows in Figure 1b). This increase was necessary because, for both of the initial concentrations of tracer used here, the EF was found to reach a plateau when E_{tot} was held constant. For example, in the enrichment of 1.0 nM $BODIPY^{2-}$ at $E_{tot} = 200$ V, a plateau at EF = 25 000 is apparent after 1000 s (Figure 1b). A similar plateau is observed with an initial concentration of 10.0 pM tracer; however, it is not shown in Figure 1b because the plateau is typically reached just after 2000 s of enrichment (See Supporting Information). Increasing E_{tot} too rapidly results in formation of gas bubbles at the BPE cathode.

The EF observed under these conditions is 3 orders of magnitude higher than what has been reported for BPE focusing thus far.[1,2,4,5] The conditions used here were optimized on the basis of our previously published study of the fundamental parameters affecting the enrichment process.[1,3] Specifically, optimization was accomplished by adjusting experimental parameters determining the standard deviation (s) of the width of the focused band (eq 6).[40]

$$s = \sqrt{\frac{D_{im} + \left(\frac{u_{eo,l}}{u_m} - 1\right)^2 \frac{a^2 {u_m}^2}{52.5 D_{im}}}{|\mu_{ep} m|}} \qquad (6)$$

Here, a is the half-height of a 2-D (parallel plate) rectangular channel, m is the slope of the electric field gradient, u_m is the mean convective flow velocity of the solution, $u_{eo,l}$ is the local electroosmotic flow velocity in the depletion zone, and D_{im} and μ_{ep} are, respectively, the diffusion coefficient and electrophoretic mobility of the focused species. The EFs in Figure 1b are orders of magnitude higher than previously reported for the following reasons. First, the channel height (a) was decreased from 21 to 1.6 μm, which directly decreases s. Second, a higher buffer concentration was employed, which has been shown to increase m and the enrichment rate.[1] It was not possible to use higher buffer concentrations in channels with higher cross sectional areas due to high current densities in the BPE and corresponding gas bubble formation. In the 1.6 μm-high channel, however, the current density at the BPE is greatly decreased (vide infra), which suppresses bubble formation. Finally, the BPE was shortened allowing use of higher E_{tot}, thereby further increasing m and the enrichment rate.[1]

Determination of Faradaic Current in a Single-Channel Configuration. In the preceding subsection, we alluded to a decrease in current density in the BPE when channels having a smaller cross sectional area are used. Here, we quantitatively address the relationship between i_{BPE} and E_{tot} for channels having dimensions of 21 μm high by 100 μm wide and 1.6 μm high by 10 μm wide. Current measurement experiments were performed with each channel size using the following procedure. First, the channels were rinsed with buffer and then refilled with fresh buffer as described in the Experimental Section. Second, the two halves of the 100 μm long split BPE were connected with an ammeter. Finally, a driving voltage (E_{tot} = 20.0−800 V) was applied for 30 s while i_{BPE} was recorded. This procedure was repeated three times for each value of E_{tot} allowing 30 s between measurements. Values of i_{BPE} taken at the end of each of the three cycles (at which time i_{BPE} had attained a stable value) were then averaged.

Figure 1e,f shows the resulting i_{BPE} vs E_{tot} behavior. First, consider the data taken using 100 mM Tris in a 1.6 μm high channel (the same conditions as those used for enrichment in Figure 1b). Below $E_{tot} = 100$ V, ΔE_{elec} is not sufficiently high to drive water electrolysis at the ends of the BPE and i_{BPE} increases gradually. This increase is most likely due to O_2 reduction at the BPE cathode and water oxidation (eq 3) at the BPE anode. However, between $E_{tot} = 100$ and 200 V ($\Delta E_{elec} = 1.6$ and 3.3 V), i_{BPE} steps to a higher value. This corresponds to the onset of water electrolysis. Above $E_{tot} = 200$ V, i_{BPE} continues to increase.

The value of i_{BPE} is determined by several factors including the total current in the microchannel (limited by ionic strength). Therefore, at low buffer concentration (10 mM Tris, 1.6 μm-high channel), the current at all values of E_{tot} is less than 100 pA (Figure 1f). In contrast to the results for the 1.6 μm-high channel, it was not possible to obtain values for i_{BPE} in the 21 μm high channel containing 10.0 or 100.0 mM Tris for $E_{tot} > 200$ V and $E_{tot} > 100$ V, respectively, because gas bubbles formed at the BPE under these conditions.

The i_{BPE} results for 21 and 1.6 μm-high channels qualitatively demonstrate lower current density in the smaller channel. However, a quantitative comparison requires that values of i_{BPE} must be obtained under similar conditions. This situation is fulfilled when $E_{tot} = 200$ V and the electrolyte is 10.0 mM Tris. Under these conditions, the values of i_{BPE} for the 21 and 1.6 μm-high channels are 258 ± 5 nA (Figure 1e) and 29.0 ± 0.3 pA (Figure 1f), respectively. These currents correspond to current

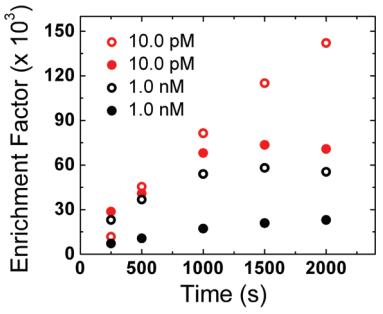

Figure 2. Plot of enrichment factor versus time obtained using the dual channel device illustrated in Scheme 2a. Solutions contained 10.0 pM (red) or 1.0 nM (black) $BODIPY^{2-}$ in 100 mM Tris·$HClO_4$ (pH 8.1). VP 2 (filled circles) and VP 3 (open circles; Table 1) were applied to drive enrichment.

densities of 7.37 mA/cm^2 and 8.29 μA/cm^2, respectively. Note, however, that division of i_{BPE} by the total area of one side of the split BPEs provides only a rough estimate of the current density. The actual distribution of current along the BPE is nonuniform, with high current density at the distal edges of the electrode.[43] Nevertheless, the current density in the smaller channel is estimated to be ~1000 times lower than in the larger channel under the same conditions. Because of this lower current density, gas bubble formation is suppressed in the 1.6 μm high channel.

Enrichment of $BODIPY^{2-}$ in a Dual-Channel Configuration. The enrichment of 10.0 pM and 1.0 nM $BODIPY^{2-}$ was carried out using the dual-channel configuration discussed earlier (Scheme 2a). Prior to enrichment, both channels were rinsed as described in the Experimental Section. Then, the contents of the reservoirs were replaced with fresh 100 mM Tris (pH 8.1) containing 10.0 pM or 1.0 nM $BODIPY^{2-}$. Finally, either VP 2 or VP 3 (Table 1) was applied to initiate enrichment. Enrichment was carried out for 2000 s.

The time-dependent enrichment of the resulting focused band of tracer is shown in Figure 2. With an initial tracer concentration of 1.0 nM, and using VP 2, enrichment reaches 23 000-fold in 2000 s at an average rate of 9.3-fold/s. This rate of enrichment is similar to that observed for the same tracer concentration during the first 2000 s of enrichment in the single-channel configuration (Figure 1b). Using VP 3, but otherwise the same conditions, the tracer enriches 55 000-fold at an average rate of 27-fold/s. An additional increase in EF is observed for both VP 2 and VP 3 when the initial concentration of tracer is lowered to 10.0 pM. For example, VP 2 results in 71 000-fold enrichment (36-fold/s), and VP 3 leads to 142 000-fold enrichment (71-fold/s). The latter is the highest rate of enrichment we have reported thus far.[1,2,4,5] Typical EFs and rates reported for some other CFGF methods are EF = 10 000 at 1.7-fold/s for TGF[26] and EF = 10 000 at 4.17-fold/s for EFGF.[27] Wang et al. achieved enrichment rates ranging from 0.125 fold/s to 4170 fold/s for 33 nM and 33 fM analyte concentrations, respectively.[38] However, the most comparable initial concentration they reported was 33 pM, for which the enrichment rates was ~28-fold/s. This is somewhat lower than we observed under similar conditions: 71-fold/s for an initial analyte concentration of 10.0 pM.

The reasons for attainment of higher enrichment factors at lower initial tracer concentrations has been reported and discussed previously by us[1,3] and others.[38] Briefly, a higher tracer concentration contributes to the ionic strength at the depletion zone boundary, thereby degrading the electric field gradient.[1,3] Unfortunately, our current fluorescence measurement system does not provide sufficient contrast for initial concentrations lower than 10 pM, and therefore, it was not possible to access even higher enrichment factors by starting with femtomolar tracer concentrations. The gain in enrichment rate observed for VP 3 compared to VP 2 is due to the increase in E_{tot}. This dependence on E_{tot} is similar to that described earlier for the single-microchannel arrangement.[1] That is, an increase in the electric field strength in the focusing channel accelerates transport of the tracer from the anodic reservoir to the focusing location, increases both forces responsible for focusing (electromigration of the tracer and opposing convective flow driven by electroosmosis, Scheme 1d), and increases the slope of the electric field gradient.[1] Most importantly, in the dual-channel configuration, E_{tot} can be increased while maintaining ΔE_{elec} at a sufficiently low value to prevent gas bubble formation and degradation of the BPE. In the single-channel configuration, however, as E_{tot} increases, ΔE_{elec} increases proportionally (Scheme 1c).

In addition to the ion depletion zone present at the BPE cathode, faradaic ICP is also expected to generate an ion enrichment zone at the BPE anode. Qualitative evidence for this is provided by dual-channel studies employing a 100 μm-wide BPE connecting two 20 μm-high, 100 μm-wide channels. In this experiment, both channels were filled with 10.0 mM Tris (pH 8.1) and 0.1 μM $BODIPY^{2-}$, and upon application of VP 4, the tracer in the auxiliary channel was observed to enrich directly over the BPE anode. Further characterization of the depletion and enrichment zones will be the focus of future studies.

Measurement of i_{BPE} and ΔE_{elec} in the Dual-Channel Configuration. In the dual-channel system, i_{BPE} and ΔE_{elec} were measured using VP 2 and VP 3 (Table 1) and a procedure that is discussed in the Supporting Information. Using VP 2, i_{BPE} = 188 ± 3 nA, and using VP 3, i_{BPE} = 386 ± 4 nA. Two important conclusions can be drawn from these results. First, the existence of a stable, nonzero value of i_{BPE} supports the foregoing discussion regarding the underlying phenomena governing the behavior of the dual channel system. Specifically, a potential difference (ΔE_{elec}) is established across the BPE between the focusing and auxiliary channels (Scheme 2a,b), leading to faradaic reactions at the BPE ends and current flow (i_{BPE}) between the channels. Second, the magnitude of i_{BPE} (hundreds of nanoamps) is similar to that observed for a single-channel device (blue circles, Figure 1e) having the same channel height (1.6 μm) and filled with the same buffer concentration (100 mM Tris). This is important, because the magnitude of i_{BPE} is a measure of the rate of faradaic reactions, which in turn governs the rate of formation and magnitude of the ion depletion zone.

The measured values for ΔE_{elec} were ~11 and ~8 V for VP 2 and VP 3, respectively. These are rough estimates, but they highlight the advantage of the dual-channel configuration. Specifically, consider that when changing from VP 2 to VP 3, E_{tot} increases by a factor of 1.5 from 200 to 300 V. In a single-channel configuration, such an increase in E_{tot} would produce a 1.5-fold increase in ΔE_{elec}. However, no such increase is observed in the dual-channel system. Furthermore, if ΔE_{elec} is ever found to be too high, it can be adjusted to a lower value by simply increasing V_3 and V_4 (Scheme 2a). The decoupling of E_{tot} and ΔE_{elec} is one of the key advantages of the dual channel configuration.

SUMMARY AND CONCLUSIONS

We have demonstrated that faradaic processes at the ends of a BPE connecting two microchannels can generate enrichment

and depletion zones. This faradaic ICP is similar to traditional ICP at micro/nanochannel junctions but employs a much simpler device architecture. In the present study, we described the use of an ion depletion zone to form a steep electric field gradient, and this led to focusing of a fluorescent tracer in both a single and dual-channel configuration. The dual-channel configuration provides a significantly higher rate of enrichment (71-fold/s vs 28-fold/s) for a given initial concentration of analyte (~10 pM) than has been reported for ICP induced at the intersection of a micro- and nanoscale channel.[38] In the future, we plan to expand our study of faradaic ICP to include other pairs of faradaic reactions that more closely mimic traditional ICP behavior. This will allow us to directly compare the two methods and perhaps better understand the propagation of the enrichment and depletion zones in traditional ICP.[47] We are also developing methods for detecting the presence of the enriched bands using electrochemical methods rather than fluorescence. The results of these studies will be reported in due course.

APPENDIX. Major Symbols

symbol	meaning	unit
a	half height of a rectangular channel	m
D_{im}	molecular diffusivity	m^2/s
D_u	Dukhin number	unitless
ΔE_{elec}	potential difference between two ends of the bipolar electrode	V
E^o	standard reduction potential	V
E_{tot}	applied voltage between the driving electrodes	V
i_{EDL}	ionic current through the EDL	A
i_b	ionic current through the bulk solution	A
i_{BPE}	current through the BPE	A
i_{tot}	total current through the microchannel	A
m	slope of the electric field gradient	kV/m^2
μ_{ep}	electrophoretic mobility	$cm^2/V \cdot s$
s	standard deviation of the width of a focused band	m
σ_b	ionic conductance of the bulk solution	S
σ_{EDL}	ionic conductance of the EDL	S
$u_{eo,l}$	local electroosmotic velocity	cm/s
u_m	mean convective flow velocity	cm/s

ASSOCIATED CONTENT

Supporting Information. The devices and protocols used to measure i_{BPE} and ΔE_{elec} using the dual-channel microfluidic configuration; the plateau in EF during enrichment of 10.0 pM $BODIPY^{2-}$ in the single-channel configuration (E_{tot} = 200 V). This material is available free of charge via the Internet at http://pubs.acs.org.

AUTHOR INFORMATION

Corresponding Author
*E-mail: crooks@cm.utexas.edu.

ACKNOWLEDGMENT

We gratefully acknowledge support from the Chemical Sciences, Geosciences, and Biosciences Division, Office of Basic Energy Sciences, Office of Science, U.S. Department of Energy (Contract No. DE-FG02-06ER15758). We also thank the Robert A. Welch Foundation (Grant F-0032) for sustained support. This material is based in part upon work supported under a National Science Foundation Graduate Research Fellowship awarded to R.K.A..

REFERENCES

(1) Anand, R. K.; Sheridan, E.; Hlushkou, D.; Tallarek, U.; Crooks, R. M. *Lab Chip* **2011**, *11*, 518−527.
(2) Dhopeshwarkar, R.; Hlushkou, D.; Nguyen, M.; Tallarek, U.; Crooks, R. M. *J. Am. Chem. Soc.* **2008**, *130*, 10480–10481.
(3) Hlushkou, D.; Perdue, R. K.; Dhopeshwarkar, R.; Crooks, R. M.; Tallarek, U. *Lab Chip* **2009**, *13*, 1903–1913.
(4) Laws, D. R.; Hlushkou, D.; Perdue, R. K.; Tallarek, U.; Crooks, R. M. *Anal. Chem.* **2009**, *81*, 8923–8929.
(5) Perdue, R. K.; Laws, D. R.; Hlushkou, D.; Tallarek, U.; Crooks, R. M. *Anal. Chem.* **2009**, *81*, 10149–10155.
(6) Chiu, D. T. *Anal. Bioanal. Chem.* **2010**, *397*, 3179–3183.
(7) Tia, S.; Herr, A. E. *Lab Chip* **2009**, *9*, 2524–2536.
(8) Borland, L. M.; Kottegoda, S.; Phillips, K. S.; Allbritton, N. L. *Annu. Rev. Anal. Chem.* **2008**, *1*, 191–227.
(9) Bocquet, L.; Charlaix, E. *Chem. Soc. Rev.* **2010**, *39*, 1073–1095.
(10) Kovarik, M. L.; Jacobson, S. C. *Anal. Chem.* **2009**, *81*, 7133–7140.
(11) Lorenz, R. M.; Chiu, D. T. *Acc. Chem. Res.* **2009**, *42*, 649–658.
(12) Theberge, A. B.; Courtois, F.; Schaerli, Y.; Fischlechner, M.; Abell, C.; Hollfelder, F.; Huck, W. T. S. *Angew. Chem., Int. Ed.* **2010**, *49*, 5846–5868.
(13) Ohno, K.; Tachikawa, K.; Manz, A. *Electrophoresis* **2008**, *29*, 4443–4453.
(14) Song, S.; Singh, A. *Anal. Bioanal. Chem.* **2006**, *384*, 41–43.
(15) Mavré, F.; Anand, R. K.; Laws, D. R.; Chow, K.-F.; Chang, B.-Y.; Crooks, J. A.; Crooks, R. M. *Anal. Chem.* **2010**, *82*, 8766–8774.
(16) Shackman, J. G.; Ross, D. *Electrophoresis* **2007**, *28*, 556–571.
(17) Cui, H.; Horiuchi, K.; Dutta, P.; Ivory, C. F. *Anal. Chem.* **2005**, *77*, 1303–1309.
(18) Hofmann, O.; Che, D.; Cruickshank, K. A.; Müller, U. R. *Anal. Chem.* **1998**, *71*, 678–686.
(19) Li, C.; Yang, Y.; Craighead, H. G.; Lee, K. H. *Electrophoresis* **2005**, *26*, 1800–1806.
(20) Lichtenberg, J.; Verpoorte, E.; de Rooij, N. F. *Electrophoresis* **2001**, *22*, 258–271.
(21) Yang, H.; Chien, R.-L. *J. Chromatogr., A* **2001**, *924*, 155–163.
(22) Gebauer, P.; Boček, P. *Electrophoresis* **2002**, *23*, 3858–3864.
(23) Jung, B.; Bharadwaj, R.; Santiago, J. G. *Anal. Chem.* **2006**, *78*, 2319–2327.
(24) Balss, K. M.; Vreeland, W. N.; Phinney, K. W.; Ross, D. *Anal. Chem.* **2004**, *76*, 7243–7249.
(25) Hoebel, S. J.; Balss, K. M.; Jones, B. J.; Malliaris, C. D.; Munson, M. S.; Vreeland, W. N.; Ross, D. *Anal. Chem.* **2006**, *78*, 7186–7190.
(26) Ross, D.; Locascio, L. E. *Anal. Chem.* **2002**, *74*, 2556–2564.
(27) Humble, P. H.; Kelly, R. T.; Woolley, A. T.; Tolley, H. D.; Lee, M. L. *Anal. Chem.* **2004**, *76*, 5641–5648.
(28) Koegler, W. S.; Ivory, C. F. *J. Chromatogr., A* **1996**, *726*, 229–236.
(29) Lin, S.-L.; Li, Y.; Tolley, H. D.; Humble, P. H.; Lee, M. L. *J. Chromatogr., A* **2006**, *1125*, 254–262.
(30) Lin, S.-L.; Li, Y.; Woolley, A. T.; Lee, M. L.; Tolley, H. D.; Warnick, K. F. *Electrophoresis* **2008**, *29*, 1058–1066.
(31) Meighan, M. M.; Staton, S. J. R.; Hayes, M. A. *Electrophoresis* **2009**, *30*, 852–865.
(32) Sun, X.; Farnsworth, P. B.; Tolley, H. D.; Warnick, K. F.; Woolley, A. T.; Lee, M. L. *J. Chromatogr., A* **2009**, *1216*, 159–164.
(33) Burke, J. M.; Huang, Z.; Ivory, C. F. *Anal. Chem.* **2009**, *81*, 8236–8243.

(34) Burke, J. M.; Smith, C. D.; Ivory, C. F. *Electrophoresis* **2010**, *31*, 902–909.
(35) Huang, Z.; Ivory, C. F. *Anal. Chem.* **1999**, *71*, 1628–1632.
(36) Höltzel, A.; Tallarek, U. *J. Sep. Sci.* **2007**, *30*, 1398–1419.
(37) Kim, S. M.; Burns, M. A.; Hasselbrink, E. F. *Anal. Chem.* **2006**, *78*, 4779–4785.
(38) Wang, Y.-C.; Stevens, A. L.; Han, J. *Anal. Chem.* **2005**, *77*, 4293–4299.
(39) Zhou, K.; Kovarik, M. L.; Jacobson, S. C. *J. Am. Chem. Soc.* **2008**, *130*, 8614–8616.
(40) Maynes, D.; Tenny, J.; Webb, B. W.; Lee, M. L. *Electrophoresis* **2008**, *29*, 549–560.
(41) McDonald, J. C.; Duffy, D. C.; Anderson, J. R.; Chiu, D. T.; Wu, H.; Schueller, O. J. A.; Whitesides, G. M. *Electrophoresis* **2000**, *21*, 27–40.
(42) Arora, A.; Eijkel, J. C. T.; Morf, W. E.; Manz, A. *Anal. Chem.* **2001**, *73*, 3282–3288.
(43) Mavré, F.; Chow, K.-F.; Sheridan, E.; Chang, B.-Y.; Crooks, J. A.; Crooks, R. M. *Anal. Chem.* **2009**, *81*, 6218–6225.
(44) Ordeig, O.; Godino, N.; del Campo, J.; Munoz, F. X.; Nikolajeff, F.; Nyholm, L. *Anal. Chem.* **2008**, *80*, 3622–3632.
(45) Kim, S. J.; Song, Y.-A.; Han, J. *Chem. Soc. Rev.* **2010**, *39*, 912–922.
(46) Zangle, T. A.; Mani, A.; Santiago, J. G. *Chem. Soc. Rev.* **2010**, *39*, 1014–1035.
(47) Zangle, T. A.; Mani, A.; Santiago, J. G. *Langmuir* **2009**, *25*, 3909–3916.